Int. J. Heat Mass Transfer. Vol. 35, No. 9, pp. 2119–2130, 1992
Printed in Great Britain

0017–9310/92 $5.00 + 0.00

Convection in an asymmetrically heated cylinder

J. P. PULICANI,† S. KRUKOWSKI,‡ J. IWAN D. ALEXANDER, J. OUAZZANI and F. ROSENBERGER

Center for Microgravity and Materials Research, University of Alabama in Huntsville, Huntsville, AL 35899, U.S.A.

(*Received* 4 *April* 1991 *and in final form* 6 *September* 1991)

Abstract—Recently, non-axisymmetric convection in vertical directional solidification experiments has been observed. It has been suggested that the asymmetry is due to lack of azimuthal symmetry in imposed temperature and that the flow asymmetry will decrease with increasing velocities. Motivated by these observations we have examined the consequences of deviations from axisymmetric wall temperature conditions in a vertical differentially heated cylinder. We show that the degree of flow asymmetry depends on the ratio, A_0, between the amplitudes of the maximum azimuthal and vertical temperature differences, and that for a fixed value of this ratio the flow asymmetry increases with increasing flow velocity (Rayleigh number).

1. INTRODUCTION

THE CHARACTER of convection during solidification has been examined using numerical models of buoyancy-driven convection in cylindrical and rectangular geometries. Early work examined a variety of imposed temperature boundary conditions [1–7]. These range from purely vertical temperature gradients which result in convection after a critical value of the Rayleigh number is exceeded [4–6], to idealized conditions associated with Bridgman–Stockbarger furnaces [3] which are imposed directly on the melt and crystal without consideration of the heat transfer between the ampoule, furnace and sample. For these boundary conditions, flow always occurs owing to the presence of radial temperature gradients. Later models have accounted for the presence of the ampoule and the details of furnace design [8, 9]. In practice, the thermal profile of the inner surface of the furnace is not realized at the ampoule wall; it is modified by heat transfer between the crystal, melt, ampoule and the furnace itself. The tendency is to reduce axial temperature gradients, while radial temperature gradients may increase or decrease depending on the specific nature of the heat transfer between the crystal, melt and ampoule [8]. Crespo del Arco and Bontoux [10] studied the occurrence of asymmetric flows in cylindrical cavities. These studies were restricted to cases for which the thermal boundary conditions possessed azimuthal symmetry.

Recently, non-axisymmetric convection has been observed in directional solidification experiments conducted with low melting point, low thermal conductivity materials [11, 12]. Potts and Wilcox [11] suggested that the flows observed in their experiments were due to lack of azimuthal symmetry in the temperature field caused by the fact that the particular Bridgman–Stockbarger soldification apparatus precluded any control of the azimuthal temperature field. Neugebauer and Wilcox [12] quantitatively investigated flow symmetries during Bridgman–Stockbarger solidification of salol using an experimental system which allowed control of the azimuthal temperature variations.

In many cases, thermal asymmetries in Bridgman-type systems may arise owing to the difficulties involved with constructing an axisymmetric heating arrangement and in aligning the ampoule axis with the axis of the furnace. During growth of high temperature materials, any misalignment of the ampoule will result in an azimuthal variation in the radiation view factors for the ampoule. This will lead to asymmetry in the temperature of the ampoule wall.

In this work we examine the character of convection in an asymmetrically heated cylindrical ampoule using an idealized model of a Bridgman-type configuration. The object is to identify trends in the flow behavior (rather than attempt to accurately model the experiments of Neugebauer and Wilcox [12]) and in particular to investigate whether conclusions drawn from their experiments apply at lower Prandtl numbers. A much simpler system is examined in which the temperature is an increasing function of height (in ref. [12] the temperature has a maximum in the melt at some distance above the solid–liquid interface and subsequently decreases with height). We also impose a well-defined thermal asymmetry. In Section 2 we formulate the model problem. In Section 3 we outline the pseudospectral collocation method used to solve the 3D problem. The results are presented in Section 4 and discussed in Section 5.

† Present address: Département de Mathématiques et Mécanique, case 322, Faculté des Sciences et Techniques, Av. Escadrille Normandie-Niemen, 13397 Marseille Cedex 13, France.

‡ Present address: High Pressure Research Center, Polish Academy of Sciences, Sokolowska 29/37 01-142, Warsaw, Poland.

NOMENCLATURE

A	aspect ratio, $2H/D$
A_0	parameter of A_θ
A_θ	dimensionless ΔT_θ
D	diameter
g	acceleration due to gravity
Gr	Grashof number, Ra/Pr
H	half of the cylinder height
$\mathbf{k}$	unit vector in the z-direction
N_r, N_θ, N_z	number of collocation points in the r-, θ- and z-directions respectively
Pr	Prandtl number, ν/κ
r, θ, z	cylindrical coordinates
Ra	Rayleigh number, $g\alpha H^3(T_H - T_M)/\kappa\nu$
$Re_{*\max}$	Reynolds number connected to the velocity $\bar{v}_{*\max}$, $\bar{v}_{*\max}D/\nu$; '*' corresponds to the coordinate directions (i.e. r, z, θ, x or y)
t	time
T_M, T_H	temperature at the lower and upper end walls respectively ($T_M < T_H$)
$v_{*\max}$	maximum value of v_*
$\mathbf{V}, T, p$	velocity, temperature, pressure
v_r, v_θ, v_z	radial, azimuthal and vertical components of the velocity
v_x, v_y	velocities in Cartesian coordinates such that $v_x = v_r\cos\theta - v_\theta\sin\theta$, and $v_y = v_r\sin\theta + v_\theta\cos\theta$
x, y	Cartesian coordinates
Z_a	z-coordinate of the location of the upper limit of the adiabatic zone.

Greek symbols

δt	time step
ΔT_θ	maximum azimuthal deviation in temperature
ν, κ, α	kinematic viscosity, thermal diffusivity, thermal expansion coefficient
Ω	domain of the cylinder.

2. FORMULATION OF THE PROBLEM

A practical Bridgman–Stockbarger set-up such as that decribed by Dahkoul *et al.* [13] consists of three distinct thermal zones. The simplest arrangement has a hot zone (in which, ideally, the temperature at the wall and in the melt should be almost isothermal) and a cold zone. These are separated by a gradient zone in which a thermal barrier controls the heat transfer between the ampoule and the hot and cold zones. The basic Bridgman–Stockbarger model used here is shown in Fig. 1. The fluid is differentially heated in a vertical cylinder having a height $2H$ and a diameter D. The lower and upper end walls of the cylinder are maintained at constant temperatures T_M and T_H respectively (where $T_M < T_H$). In this system the presence of the thermal barrier is approximated by taking the cylinder walls to be adiabatic in the gradient zone. In the hot zone we impose asymmetry in the temperature distribution using a function which causes azimuthal and vertical deviations from isothermal conditions on the cylinder wall. The maximum azimuthal deviation in temperature is given by ΔT_θ (see Fig. 1). All boundaries of the cylinder are rigid with no-slip conditions for the velocities.

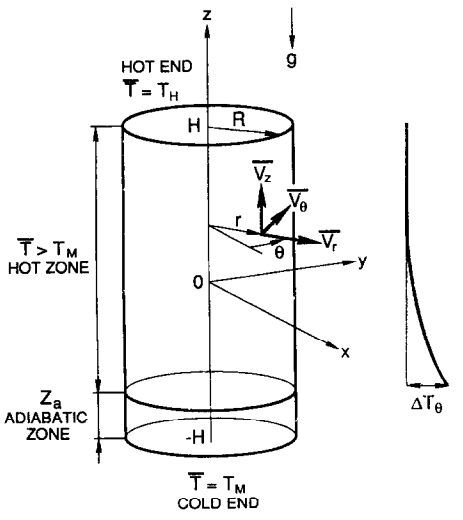

FIG. 1. Model Bridgman–Stockbarger configuration.

The equations governing energy, momentum and mass transport are written in primitive variables for cylindrical coordinates and the Boussinesq approximation is assumed. We employed H, $\nu Ra/HPr$, $\nu Ra/H^2Pr$ and $T_H - T_M$ to non-dimensionalize length, velocity, time and temperature respectively. The non-dimensional governing equations have the form

$$\frac{\partial T}{\partial t} = \frac{1}{Pr}\Delta T - \frac{Ra}{Pr}\mathbf{V}\cdot\operatorname{grad} T \tag{1}$$

$$\frac{\partial \mathbf{V}}{\partial t} = \Delta\mathbf{V} - \frac{Ra}{Pr}(\operatorname{grad}\mathbf{V})\cdot\mathbf{V} - \operatorname{grad} p + T\mathbf{k} \tag{2}$$

$$\operatorname{div}\mathbf{V} = 0, \tag{3}$$

where t is the time and $\mathbf{V} = (v_r, v_\theta, v_z)$, p and $T = (\bar{T} - T_M)/(T_H - T_M)$ respectively represent the dimensionless velocity, pressure and temperature. The unit vector in the z-direction is denoted by $\mathbf{k}$; $Pr = \nu/\kappa$ is the Prandtl number, with ν the kinematic viscosity and κ the thermal diffusivity; $Ra = g\alpha H^3(T_H - T_M)/$

$\kappa\nu$ is the Rayleigh number, with g the gravitational acceleration and α the thermal expansion coefficient.

Finally, equations (3)–(5) are to be solved as functions of the independent variables (r, θ, z) in the domain $\Omega =]0,\ 1/A[\times]0,\ 2\pi[\times]-1,\ 1[$. Here the aspect ratio A is defined as $2H/D$.

The following conditions were applied at the initial iterate $(t \leqslant 0)$:

$$v_r = v_\theta = v_z = 0 \tag{4a}$$

$$T = g(r, \theta, z) f(z), \tag{4b}$$

with

$$f(z) = \frac{1}{1-\exp(\sigma)}\left[\exp\left(\frac{\sigma(1-z)}{2}\right) - \exp(\sigma)\right] \tag{4c}$$

and

$$g(r, \theta, z) = 1 + A_0 \frac{1-z}{3}\exp\left(\frac{-2z-1}{4}\right) \times (\cos(\pi-\theta)-1)\sin^2\left(\frac{r\pi A}{2}\right). \tag{4d}$$

The function $g(r, \theta, z)$ gives the initial condition for the azimuthal variation in temperature. It is convenient to express the maximum azimuthal temperature deviation ΔT_θ as a percentage of the axial temperature difference $T_H - T_M$, i.e. $A_\theta = (\Delta T_\theta \times 100\%)/(T_H - T_M)$. Table 1 gives A_θ for different values of A_0 and different aspect ratios

$$\left(A_\theta = 2A_0\left(\frac{1-Z_a}{3}\right)\exp\left(\frac{-2Z_a-1}{4}\right)\right).$$

In order to avoid discontinuities in derivatives of the temperature at the abrupt transition between the hot zone and the adiabatic zone, the function $f(z; \sigma)$ is used. The parameter σ is chosen such that were it not for the azimuthal temperature perturbation, the dimensionless wall temperature due to $f(z; \sigma)$ would be almost equal to 1 for $z > Z_a$, where Z_a is the z-coordinate of the location of the upper limit of the adiabatic zone.

The following dimensionless boundary conditions are applied at $t > 0$:

$$v_r = v_\theta = v_z = 0 \quad \text{at } z = \pm 1 \text{ and } r = \frac{1}{A} \tag{5a}$$

$$T = 0 \quad \text{at } z = -1, \quad T = 1 \quad \text{at } z = 1 \tag{5b}$$

Table 1. Values of the percentage of azimuthal temperature difference A_θ

Aspect ratio	A_0	A_θ
1	0.1	10%
1	0.02	2%
1	0.2	20%
2	0.1	13.2%
2	0.2	26.4%

$$T = g(r, \theta, z) f(z) \quad \text{at } r = \frac{1}{A} \text{ and } z > Z_a (z \neq \pm 1) \tag{5c}$$

$$\frac{\partial T}{\partial r} = 0 \quad \text{at } r = \frac{1}{A} \text{ and } z \leqslant Z_a. \tag{5d}$$

The azimuthal temperature variation on the ampoule wall is given by $g(1/A, \theta, z)$ and is enforced only for the hot zone $z > Z_a$.

3. NUMERICAL METHOD

Equations (1)–(3) have been solved using a modified version of the Fourier–Chebyshev pseudospectral method introduced by Pulicani and Ouazzani [14]. For this method the singularity which arises at $r = 0$ when using cylindrical coordinates (without axisymmetry) is avoided by using a change of dependent variables. The singularity arises because $r = 0$ is an artificial boundary of the computational domain; i.e. it occurs only by construction of the coordinate system. The change of variables used to cope with the singularity is

$$T = \frac{\tilde{T}}{r}, \quad v_r = \frac{\tilde{v}_r}{r}, \quad v_\theta = \frac{\tilde{v}_\theta}{r}, \quad v_z = \frac{\tilde{v}_z}{r} \text{ and } p = \frac{\tilde{p}}{r}. \tag{6}$$

Application of (1)–(6) yields a system of equations with $\tilde{T}$, $\tilde{v}_r$, $\tilde{v}_z$, $\tilde{p}$ and $\tilde{v}_\theta$, as unknowns. Obviously, $\tilde{T} = \tilde{v}_r = \tilde{v}_z = \tilde{v}_\theta = \tilde{p} = 0$ at $r = 0$. These equations are then discretized with respect to time, $t = n\delta t$, by means of a second order semi-implicit scheme. The latter employs a combination of the Adams–Bashforth and Crank–Nicolson schemes, namely

$$\left(r - \frac{r\delta t}{2Pr}\Delta\right)\left(\frac{\tilde{T}^{n+1} - \tilde{T}^n}{r}\right) = \tilde{F}^{n,n-1} \tag{7}$$

$$\left(r - \frac{r\delta t}{2}\Delta\right)\left(\frac{\tilde{\mathbf{V}}^{n+1} - \tilde{\mathbf{V}}^n}{r}\right) = \tilde{G}^{n,n-1,n+1} - \delta t r\left[\operatorname{grad}\frac{\tilde{p}}{r}\right]^{n+1} \tag{8}$$

$$\left(\operatorname{div}\frac{\tilde{\mathbf{V}}}{r}\right)^{n+1} = 0, \tag{9}$$

with

$$\tilde{F}^{n,n-1} = \delta t\left[\frac{r}{Pr}\Delta\left(\frac{\tilde{T}}{r}\right) - \frac{3Ra}{2Pr}\tilde{\mathbf{V}}\cdot\operatorname{grad}\left(\frac{\tilde{T}}{r}\right)\right]^n + \frac{\delta t Ra}{2Pr}\left[\tilde{\mathbf{V}}\cdot\operatorname{grad}\left(\frac{\tilde{T}}{r}\right)\right]^{n-1}$$

and

$$\tilde{G}^{n,n-1,n+1} = \delta t\left[r\Delta\left(\frac{\tilde{\mathbf{V}}}{r}\right) - \frac{3Ra}{2Pr}\left(\operatorname{grad}\frac{\tilde{\mathbf{V}}}{r}\right)\cdot\tilde{\mathbf{V}}\right]^n + \frac{\delta t Ra}{2Pr}\left[\left(\operatorname{grad}\frac{\tilde{\mathbf{V}}}{r}\right)\cdot\tilde{\mathbf{V}}\right]^{n-1} + [\tilde{T}\mathbf{k}]^{n+1},$$

where for convenience we have defined $\tilde{\mathbf{V}} = (\tilde{v}_r, \tilde{v}_\theta, \tilde{v}_z)$.

With this method [14], problems encountered with satisfying (9) are surmounted by using artificial compressibility [15, 16]. A false time step is employed and the method is only applicable for steady solutions to the system (1)–(5). Because of the stiffness of the physical problem at low Prandtl numbers, obtaining rapid convergence with this method at high Rayleigh numbers is difficult. In order to overcome this problem, we have modified the method by introducing two iterative processes: an outer iteration which is related to each time step and an inner iteration which ensures that (9) is satisfied to some small value, $\varepsilon \ll 1$, for each outer iterative step. It is clear that for lower values of ε, this pseudo-unsteady method takes on the character of an unsteady calculation. For this reason we have used an Adams–Bashforth scheme to discretize the convective terms instead of simply taking them explicitly [14] at the instant $t = n\delta t$ in $\tilde{F}^{n,n-1}$ and $\tilde{G}^{n,n-1,n+1}$.

A generalized ADI procedure [15] is then applied to reduce the problem to the successive solution of one-dimensional problems. For clarity, we present the method only as applied to the momentum transport equation; it is readily extended to cope with the energy transport equation. At each time step the following problem is solved:

$$\left(1-\frac{\delta t}{2}\Lambda_\theta\right)\mathbf{V}^* = \tilde{G}^{n,n-1,n+1} - \delta t r\left[\operatorname{grad}\frac{\tilde{p}}{r}\right]^{n+1,\mu} \tag{10a}$$

$$\left(1-\frac{\delta t}{2}\Lambda_z\right)\mathbf{V}^{**} = \mathbf{V}^* \tag{10b}$$

$$\left(r-\frac{r\delta t}{2}\Lambda_r\right)\left(\frac{\mathbf{V}^{***}}{r}\right) = \mathbf{V}^{**} \tag{10c}$$

$$\tilde{\mathbf{V}}^{n+1,\mu+1} = \tilde{\mathbf{V}}^n + \mathbf{V}^{***} \tag{10d}$$

$$\tilde{p}^{n+1,\mu+1} = \tilde{p}^{n+1,\mu} - \lambda r\left(\operatorname{div}\frac{\tilde{\mathbf{V}}}{r}\right)^{n+1,\mu+1}, \tag{10e}$$

where λ is a strictly positive constant and μ ($\mu = 0, 1, \ldots, N_\mu$) is the subscript connected to the inner iterative process. The operator Δ occurring in (10) has been decomposed so that $\Delta = \Lambda_r + \Lambda_\theta + \Lambda_z$. Here the Λ_α are related to the independent variables r, θ and z, respectively. Note that for $\mu = 0$, $[\operatorname{grad}(\tilde{p}/r)]^{n+1,0} = [\operatorname{grad}(\tilde{p}/r)]^n$. Equation (10e) has no physical meaning until $\delta\tilde{p}^{n+1} = \tilde{p}^{n+1,\mu+1} - \tilde{p}^{n+1,\mu} = 0$ (or practically speaking, is sufficiently small). If $\delta\tilde{p}^{n+1}$ is identically zero at each time step the method is no longer pseudo-unsteady. The present way to deal with the pressure can be time consuming when the number of internal iterations N_μ is too high. However, since we seek steady solutions, the iterative process has been introduced only to help the convergence when the solution is very stiff. It is stopped as soon as the divergence of the velocity reaches a certain value ε. The maximum value of N_μ is chosen such that the convergence is obtained after a reasonable number of outer iterations. However, it should not be so high that the divergence of the velocity is ε at the beginning of the outer iteration. The optimum values of N_μ and ε will be defined in the next section. A standard Fourier–Galerkin approximation [17] is employed for the solution of (10a) while a Chebyshev-collocation method [16] is used to solve equations (10b) and (10c). The boundary conditions are introduced by replacing the right hand sides of (10b) and (10c) by the appropriate terms [14].

The energy equation is solved in the same manner as the momentum transport equations, but needs no inner iterations to satisfy the divergence equation. The solution algorithm takes the following steps:

(i) with $\tilde{T}^n$, $\tilde{T}^{n-1}$, $\tilde{\mathbf{V}}^n$ and $\tilde{\mathbf{V}}^{n-1}$ known, we deduce $\tilde{F}^{n,n-1}$ and then $\tilde{T}^{n+1}$;

(ii) we calculate $\tilde{G}^{n,n-1,n+1}$ using $\tilde{T}^{n+1}$, $\tilde{\mathbf{V}}^n$ and $\tilde{\mathbf{V}}^{n-1}$, and then finally $\tilde{\mathbf{V}}^{n+1}$ and $\tilde{p}^{n+1}$ with (10e).

In all of the results we present here, the above method requires a distribution of points such that

$$\theta_k = \frac{2\pi k}{N_\theta}, \quad k = 0, \ldots, N_\theta - 1 \tag{11a}$$

$$z_j = \cos\left(\frac{\pi j}{N_z - 1}\right), \quad j = 0, \ldots, N_z - 1 \tag{11b}$$

$$r_i = \frac{1}{2A}\left[\cos\left(\frac{\pi i}{N_r - 1}\right) + 1\right], \quad i = 0, \ldots, N_r - 1, \tag{11c}$$

with N_r, N_θ and N_z the number of collocation points between $r = 0$ and $1/A$, $\theta = 0$ and 2π, and $z = -1$ and 1, respectively.

In our discussion of the results we shall also refer to the residual of ϑ, denoted Res ϑ, which is calculated on the collocation points of $\vartheta = \{T, v_r, v_\theta, v_z\}$. Furthermore,

$$\operatorname{Res}\vartheta = \operatorname{Max}_{i,k,j}\left[\frac{|\vartheta(r_i,\theta_k,z_j)^{n+1} - \vartheta(r_i,\theta_k,z_j)^n|}{\delta t\,\vartheta(r_i,\theta_k,z_j)^{n+1}}\right], \tag{12}$$

with $i = 0, \ldots, N_r - 1$, $k = 0, \ldots, N_\theta - 1$, $j = 0, \ldots, N_z - 1$.

The variables v_x and v_y are the velocities in Cartesian coordinates such that $v_x = v_r \cos\theta - v_\theta \sin\theta$ and $v_y = v_r \sin\theta + v_\theta \cos\theta$. We denote the maximum values of v_r, v_θ, v_z, v_x and v_y by $v_{r\max}$, $v_{\theta\max}$, $v_{z\max}$, $v_{x\max}$ and $v_{y\max}$, respectively. As these maxima are calculated at the collocation points particular to each method, small differences are expected in the results.

For all the results presented in the following section, the starting condition (4b) has only been used for $Ra = 10$. For the others, the starting condition was the solution calculated with a lower Ra. The adiabatic zone covers one fourth of the cylinder's height when the aspect ratio $A = 1$ (i.e. $Z_a = -0.5$) and one eighth when $A = 2$ (i.e. $Z_a = -0.75$). The calculations have

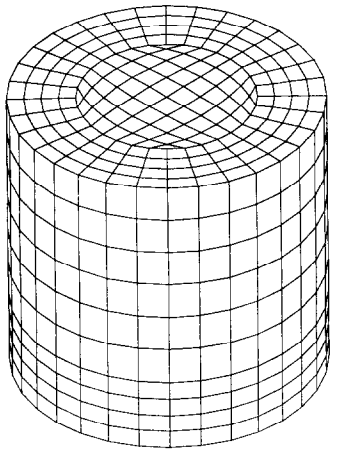

FIG. 2. Mesh used for the FIDAP calculations.

been performed on a Cray XMP/24 computer using a spatial resolution of $N_r \times N_\theta \times N_z = 13 \times 20 \times 31$ when $A = 1$ and $N_r \times N_\theta \times N_z = 13 \times 20 \times 61$ when $A = 2$. For all calculations the parameter λ of (10c) is equal to 1.3, $20 < N_\mu < 30$, and the time step δt chosen between 10^{-4} and 10^{-5} according to the stiffness of the solution. Note that we stopped the calculations when the divergence div $\mathbf{V} \approx 10^{-8}$ and Res $\mathbf{V} = 10^{-4}$. No significant change in the values of the velocity and temperature fields occurs if div $\mathbf{V}$ and Res $\mathbf{V}$ are decreased further. For the problem described here a comparison has been made between our method and the finite element code FIDAP [18, 19]. For FIDAP an irregularly spaced Cartesian grid with nodes $N_x \times N_y \times N_z = (9 \times 11 \times 31)$ was employed (see Fig. 2).

For the purpose of presenting the results we define the Reynolds number $Re_{*\max} = \bar{v}_{*\max} D/\nu$ (which is connected to the velocity), where '*' corresponds to the coordinate directions (i.e. r, z, θ, x or y).

4. RESULTS

Table 2 shows the results of a comparison between our method and the finite element code FIDAP [18, 19] for $Pr = 10^{-2}$. The values of $Re_{x\max}$, $Re_{y\max}$ and $Re_{z\max}$ were obtained with $Ra = 250$, 2500 and 15 000, $A_\theta = 20\%$ and $A = 1$. Clearly, there is good agreement between these two methods for Ra between 250 and 2500, while for $Ra = 15\,000$, the poor agreement is only due to the smaller number of points in the z-direction employed for FIDAP. Table 3 summarizes the details of our computations for $Pr = 10^{-2}$, $A = 1$, 2 and $2500 \leqslant Ra \leqslant 64\,000$, with $0 < A_\theta < 27\%$. A comparison of the velocity fields in the $\theta = 0°$ and

Table 2. Comparison between results obtained from the spectral method and from FIDAP

	Spectral			FIDAP		
Ra	$Re_{x\max}$	$Re_{y\max}$	$Re_{z\max}$	$Re_{x\max}$	$Re_{y\max}$	$Re_{z\max}$
250	10	7	20	12	8	21
2500	60	61	103	67	69	104
15 000	263	192	286	295	216	386

Table 3. Summary of the results for $Pr = 10^{-2}$

Ra	A	A_θ	δt	$Re_{r\max}$	$Re_{\theta\max}$	$Re_{z\max}$
2500	1	0	10^{-4}	70	0	122
	1	0.02	10^{-4}	69	7	120
	1	0.2	10^{-4}	61	56	103
	2	0.1	10^{-5}	69	44	114
	2	0.2	10^{-5}	69	59	125
6400	1	0.2	10^{-4}	112	123	168
	2	0.1	10^{-4}	128	99	191
15 000	1	0	10^{-4}	205	0	314
	1	0.02	10^{-4}	222	42	307
	1	0.2	10^{-4}	220	254	286
	2	0.1	10^{-5}	209	175	294
	2	0.2	10^{-5}	188	228	425
24 000	1	0	10^{-4}	242	0	384
	1	0.02	10^{-4}	267	62	376
	1	0.2	7×10^{-5}	318	363	373
64 000	1	0	10^{-4}	338	0	583

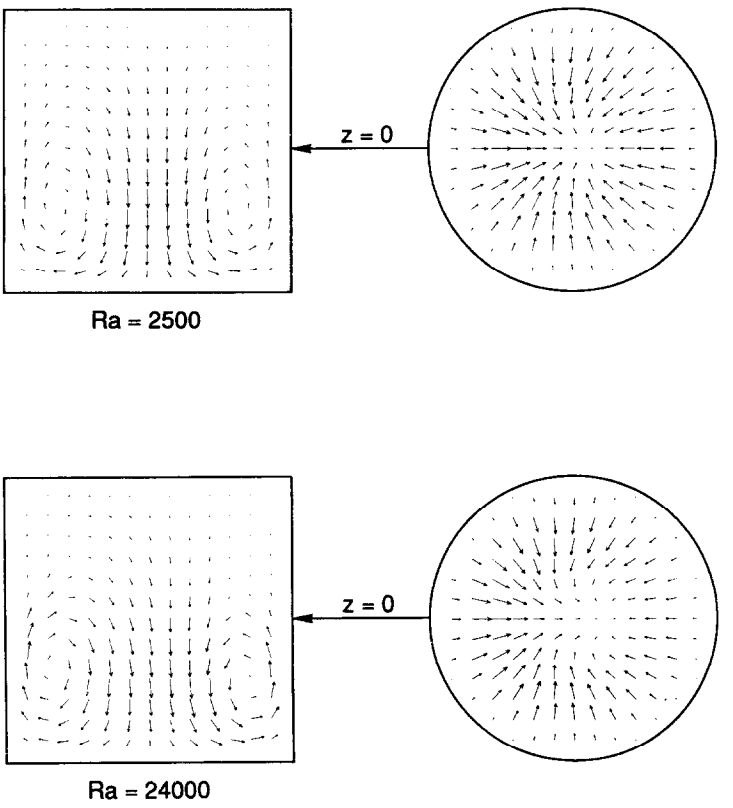

FIG. 3. Comparison of the velocity fields in the $\theta = 0°$ and 180° sections and the (r, z) plane at $z = 0$ with $A_\theta = 2\%$ and $Ra = 2500$ and 24000. Aspect ratio $A = 1$ and $Pr = 10^{-2}$.

180° sections for $A = 1$, $A_\theta = 2\%$ and $Ra = 2500$ and 24000 is given in Fig. 3. The flow asymmetry is barely perceptible at the lower Ra. Comparison of Fig. 3 with Fig. 4, which shows the velocity fields for $A = 1$, $A_\theta = 20\%$ and $Ra = 2500$, 15000 and 24000, reveals the effect of increasing the temperature asymmetry. The effect of increasing Ra at fixed A_θ is also seen in Fig. 4. Note that the locations of the roll centers change as Ra is increased. Figure 5 depicts the velocity and temperature fields for three vertical sections at $Ra = 15000$ for $A_\theta = 20\%$. Horizontal sections of the velocity field for the $Ra = 15000$ case are shown in Fig. 6.

The effect of increasing the aspect ratio is seen upon comparison of Fig. 4 with Fig. 7, which has been calculated for $Ra = 2500$ and 15000 with $A_0 = 0.2$ ($A_\theta = 26.4\%$). The basic asymmetry of the flow is not affected significantly by the increase in aspect ratio, although the centers of toroidal rolls are shifted.

Comparison of Figs. 8 and 9 for $Ra = 15000$ and $A_\theta = 13.2\%$ with Figs. 10 and 11 for $Ra = 2500$, $A_\theta = 13.2\%$ reveals that in the higher Rayleigh number case two additional cells have formed in the upper half of the cylinder. These are barely perceptible in the $Ra = 2500$ case. At higher values of A_θ these cells are able to develop well for lower values of Ra. In Fig. 7 the two-fold increase in A_θ leads to well developed upper cells even at $Ra = 2500$.

Figures 12 and 13 depict the results obtained for $Pr = 1$, $Ra = Gr = 2.5 \times 10^5$. Comparison of these results with Figs. 10 and 11 ($Pr = 10^{-2}$, $Ra = 2500$, $Gr = 2.5 \times 10^5$) reveals the effect of increasing Pr while holding the Grashof number fixed ($Gr = Ra/Pr$). There is a decrease in the degree of asymmetry in the flow for the lower Prandtl number case. The cylinder is dominated by a large asymmetric roll which extends along most of the cylinder with a smaller secondary roll along the bottom of the cylinder. The isotherms which extend into the adiabatic zone have been modified by the flow and are considerably flatter than their low Pr counterparts.

5. DISCUSSION AND SUMMARY

The results of an experimental investigation into the nature of asymmetric flow during Bridgman–Stockbarger directional solidification of salol by Neugebauer and Wilcox [12] led to the conclusion that the degree of flow asymmetry decreases with increasing convective flow velocities. Furthermore, they conjectured that for the same experimental conditions, low Prandtl number fluids exhibit correspondingly less asymmetry owing to the more rapid flow velocities which would necessarily ensue. We have carried out calculations at lower Prandtl numbers to investigate

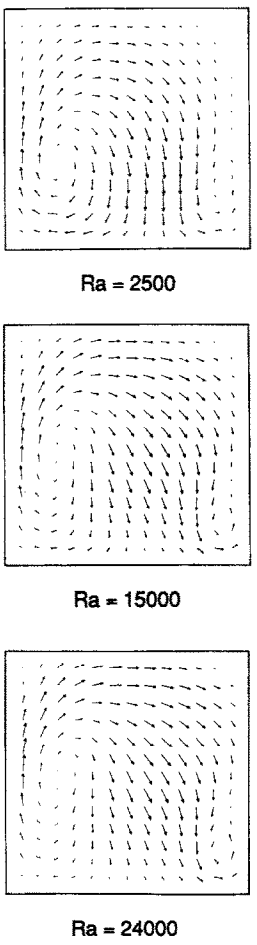

FIG. 4. Comparison of the velocity fields in the $\theta = 0°$ and 180° sections with $A_\theta = 20\%$ and $Ra = 2500$, 15000, and 24000. Aspect ratio $A = 1$ and $Pr = 10^{-2}$.

this. It can be discerned from the results presented in Section 4 that our calculations predict that for a fixed value of A_θ and Pr an increase in Ra (in practical terms caused by an increase in $\Delta T = T_H - T_M$) tends to amplify the asymmetry. Indeed, from Table 3 it can be seen that the radial and vertical velocities increase in proportion to $\sqrt{Ra}$, while the azimuthal velocity increases linearly with Ra. Examination of the experiment description and results of ref. [12] reveal that when ΔT was increased, ΔT_θ, the azimuthal variation in temperature, remained the same. In other words, the relative temperature asymmetry A_θ was decreased. Thus, the observed decrease in flow asymmetry can be explained merely by the fact that the azimuthal temperature variation was less significant for the higher Ra cases. As expected, this trend is confirmed by our calculations.

The prediction [12] that a higher Pr fluid will exhibit more asymmetry in the flow than the low Pr case is true (at least as far as the flow pattern is concerned) if the Rayleigh number is greater for the high Pr case. That the flow asymmetry is reduced due to an increase in flow velocity (Reynolds number) contradicts our results presented in Table 3 and Figs. 4–9. It is possible that for higher Rayleigh number flows than those examined here, and for temperature boundary conditions corresponding to flux conditions rather than an imposed temperature profile, the temperature asymmetry could be reduced by convective heat transport within the cylinder. In this instance an increase in flow velocity would then result in a decrease in asymmetry.

In summary, we have examined the consequences of azimuthal asymmetry in ampoule wall temperature in a differentially heated cylindrical ampoule con-

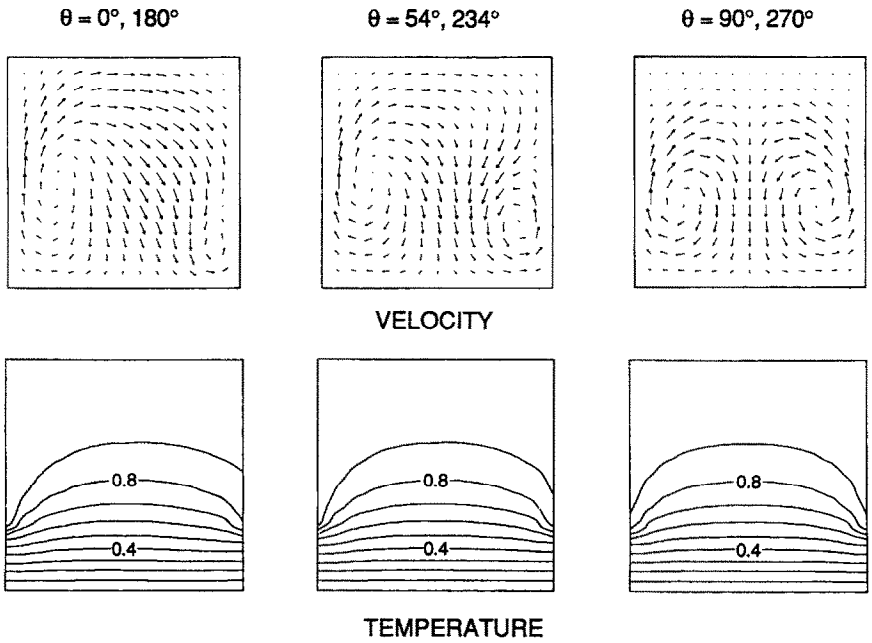

FIG. 5. Velocity and temperature fields with $A_\theta = 20\%$ and $Ra = 15000$ for $\theta = 0°$ and 180°, 54° and 234°, 90° and 270°. Aspect ratio $A = 1$ and $Pr = 10^{-2}$.

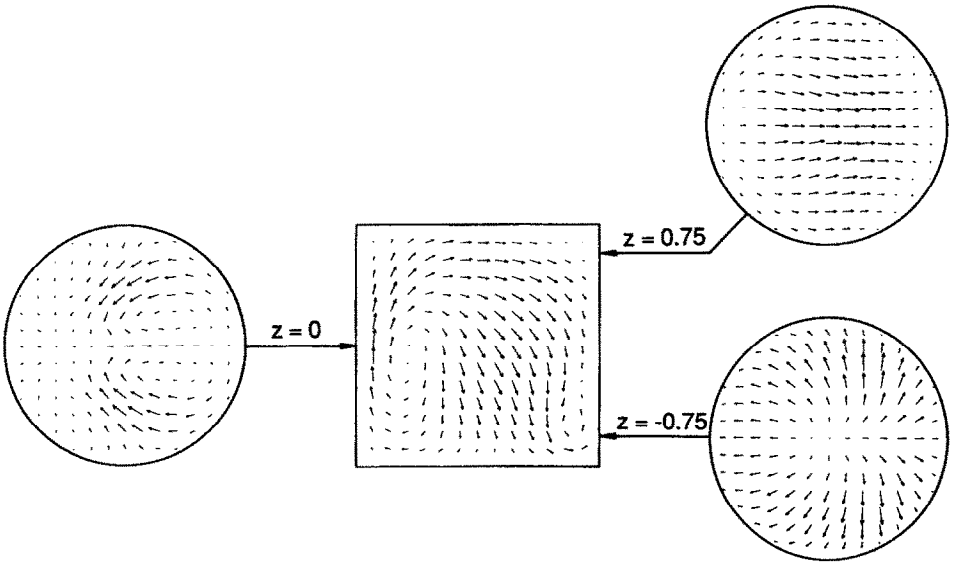

FIG. 6. Velocity field in the (r, θ) plane with $A_\theta = 20\%$ and $Ra = 15000$ at $z = 0.75$, 0, and -0.75. Aspect ratio $A = 1$ and $Pr = 10^{-2}$.

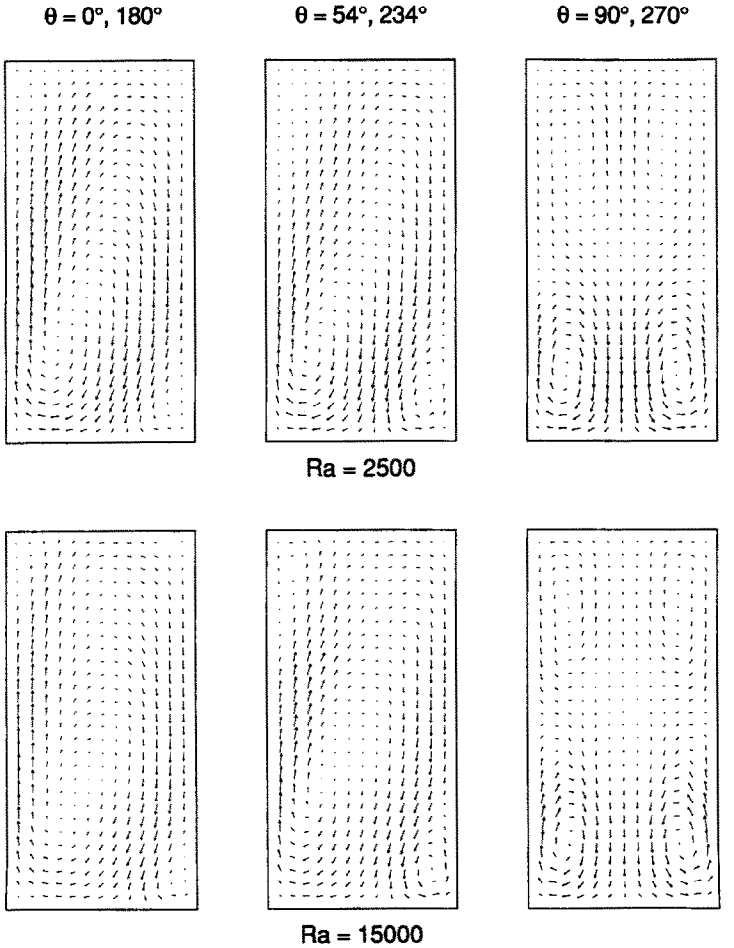

FIG. 7. Velocity fields with $A_\theta = 26.4\%$, $Ra = 2500$ and 15000 at $\theta = 0°$ and 180°, 54° and 234°, 90° and 270°. Aspect ratio $A = 2$ and $Pr = 10^{-2}$.

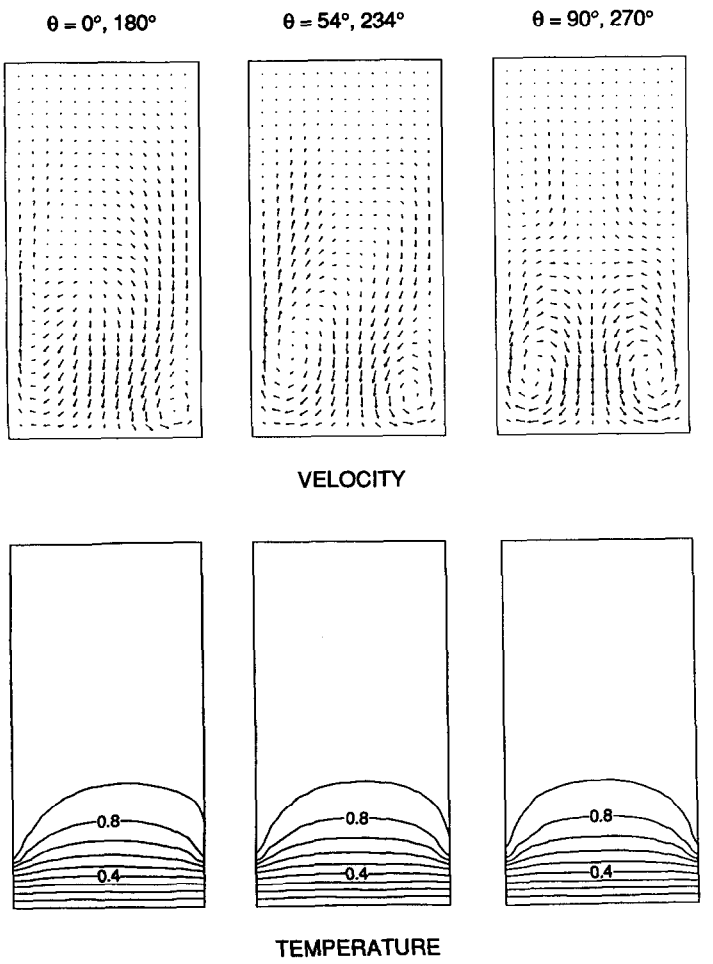

FIG. 8. Velocity and temperature fields with $A_\theta = 13.2\%$ and $Ra = 15000$ at $\theta = 0°$ and 180°, 54° and 234°, 90° and 270°. Aspect ratio $A = 2$ and $Pr = 10^{-2}$.

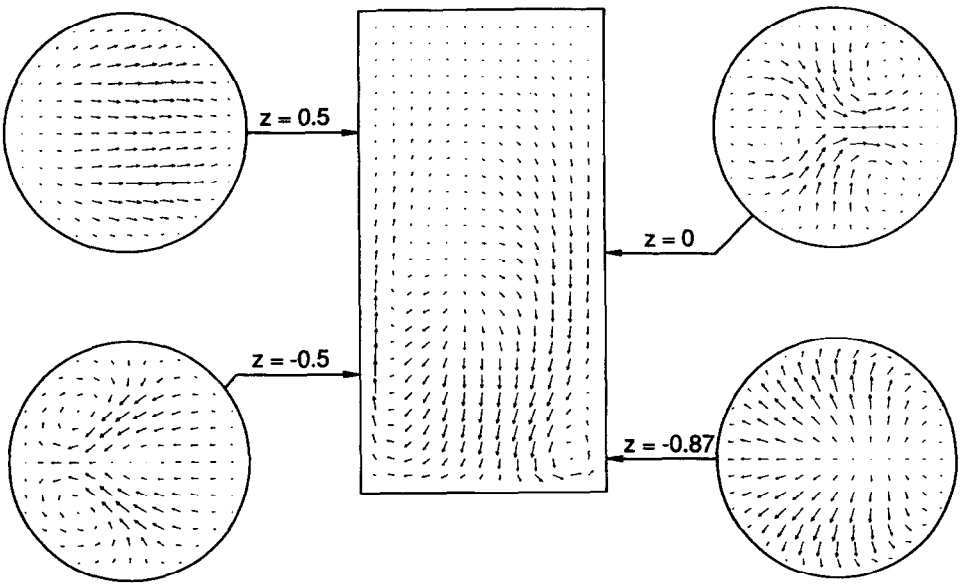

FIG. 9. Velocity field in the (r, θ) plane with $Ra = 15000$ at $z = 0.5$, 0, -0.5, and -0.87. Aspect ratio $A = 2$, $A_\theta = 13.2\%$, and $Pr = 10^{-2}$.

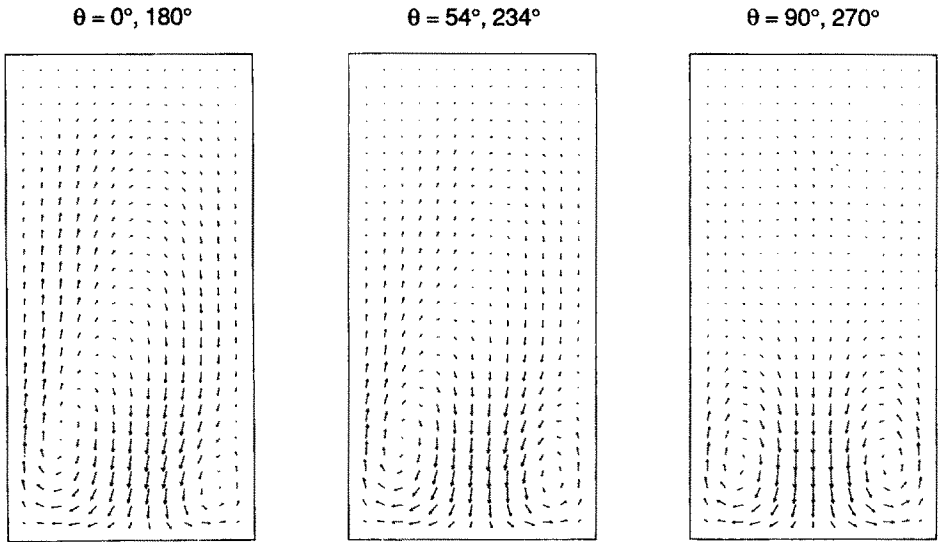

FIG. 10. Velocity field with $A_0 = 13.2\%$ and $Ra = 2500$ at $\theta = 0°$ and 180°, 54° and 234°, 90° and 270°. Aspect ratio $A = 2$ and $Pr = 10^{-2}$.

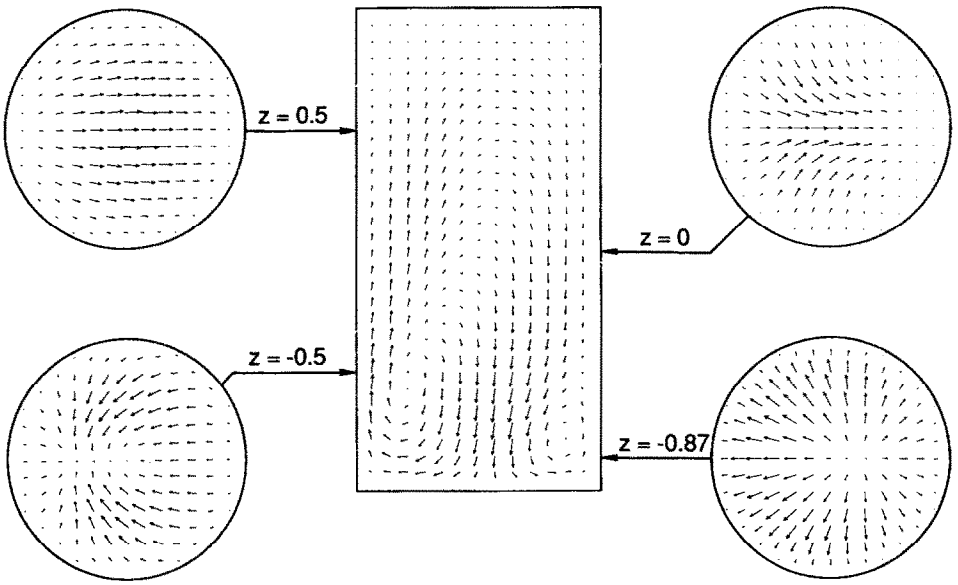

FIG. 11. Velocity field in the (r, θ) plane with $Ra = 2500$ at $z = 0.5$, 0, -0.5, and -0.87. Aspect ratio $A = 2$ and $Pr = 10^{-2}$.

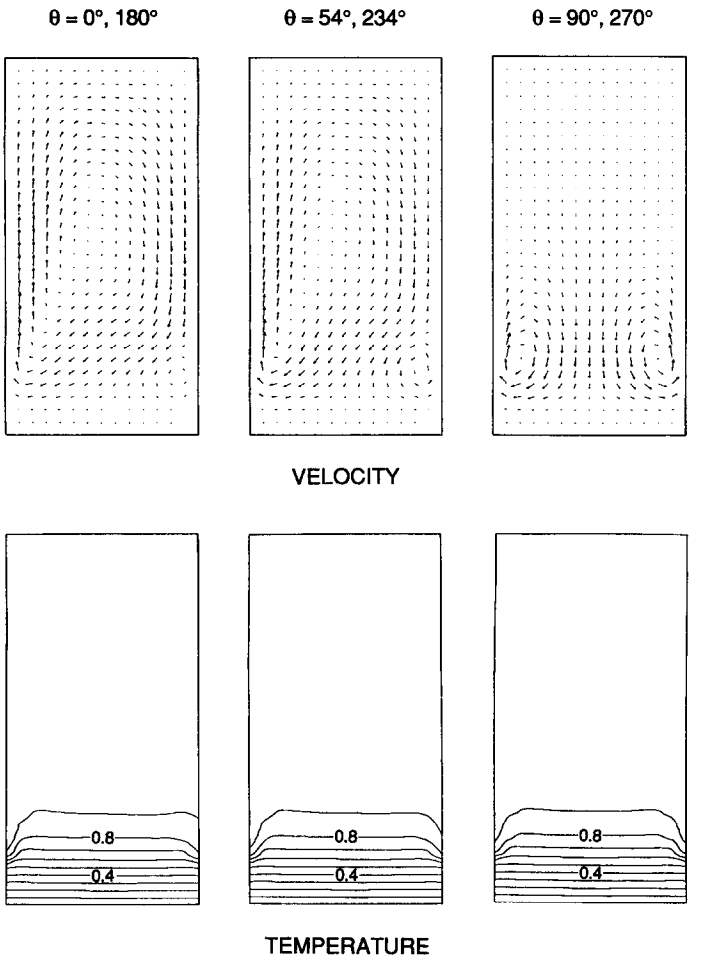

FIG. 12. Velocity and temperature fields with $A_\theta = 13.2\%$ and $Ra = 250\,000$ at $\theta = 0°$ and 180°, 54° and 234°, 90° and 270°. Aspect ratio $A = 2$ and $Pr = 1$.

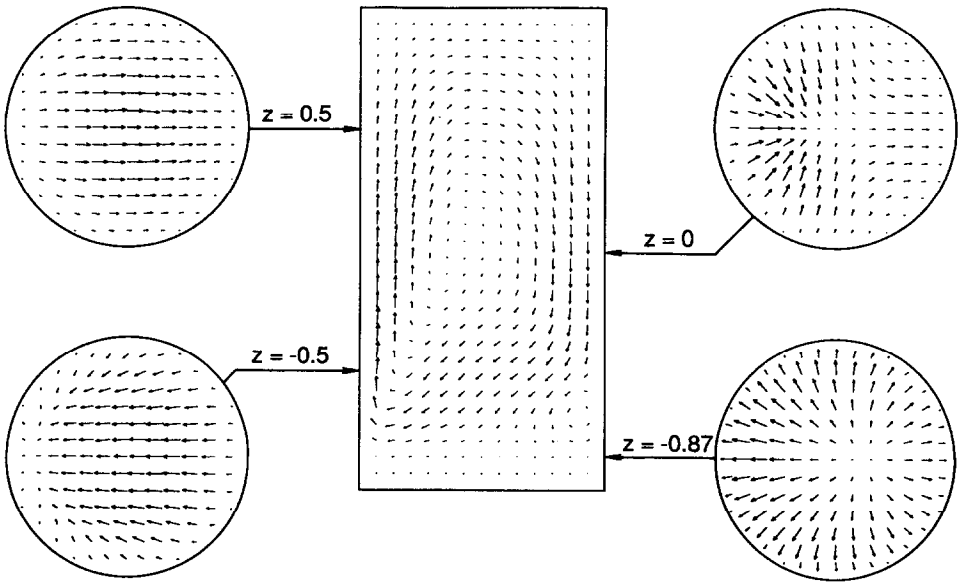

FIG. 13. Velocity field in the (r, θ) plane with $Ra = 250\,000$ at $z = 0.5$, 0, -0.5, and -0.87. Aspect ratio $A = 2$ and $Pr = 1$.

taining an incompressible Newtonian fluid. The study was motivated by recent observations of non-axisymmetric convection during directional solidification experiments conducted with low melting point, low thermal conductivity materials [11, 12]. Our results indicate that for a fixed value of the relative asymmetry in temperature A_θ, the degree of asymmetry in the flow is accentuated as the Rayleigh number is increased. For fixed Pr and Ra, the flow asymmetry increases if A_θ is increased.

Acknowledgements—This research was supported by NASA's Microgravity Science and Application Division under grants DO14 and NAG8-790, and by the state of Alabama through the Center for Microgravity and Materials Research at the University of Alabama in Huntsville and the Alabama Supercomputer Network. The authors would also like to thank M. J. B. Rogers for carefully reading the manuscript.

REFERENCES

1. P. A. Clark and W. R. Wilcox, *J. Crystal Growth* **50,** 461–469 (1980).
2. N. Kobayashi and W. R. Wilcox, *J. Crystal Growth* **59,** 616–624 (1982).
3. C. J. Chang and R. A. Brown, *J. Crystal Growth* **63,** 353–364 (1983).
4. G. Müller, in *Convective Transport and Instability Phenomena* (Edited by J. Zierep and H. Oertel), pp. 441–467. Braun-Verlag (1982).
5. G. Müller, G. Neumann and W. Weber, *J. Crystal Growth* **70,** 78–93 (1984).
6. G. Müller, *Crystals: Growth, Properties and Applications*, Vol. 12. Springer-Verlag, Berlin (1988).
7. G. B. McFadden, R. G. Rehm, S. R. Coriell, W. Clark and K. A. Morrish, *Metall. Trans.* **A15,** 2125–2135 (1984).
8. P. M. Adornato and R. A. Brown, *J. Crystal Growth* **80,** 155–190 (1987).
9. D. H. Kim, P. M. Adornato and R. A. Brown, *J. Crystal Growth* **89,** 339–356 (1988).
10. E. Crespo del Arco and P. Bontoux, *Physics Fluids* **A1,** 1348–1359 (1989).
11. H. Potts and W. R. Wilcox, *J. Crystal Growth* **73,** 350–358 (1985).
12. G. T. Neugebauer and W. R. Wilcox, *J. Crystal Growth* **89,** 143–154 (1988).
13. Y. M. Dahkoul, R. Farmer, S. L. Lehoczky and F. R. Szofran, *J. Crystal Growth* **86,** 49–55 (1988).
14. J. P. Pulicani and J. Ouazzani, A Fourier–Chebyshev pseudospectral method for solving steady 3-D Navier–Stokes and heat equations in cylindrical cavities, *Comput. Fluids* **20,** 93–109 (1991).
15. R. Peyret and T. D. Taylor, *Computational Methods for Fluid Flow*. Springer-Verlag, New York (1983).
16. J. Ouazzani and R. Peyret, *Proceedings of the 5th GAMM Workshop* (Edited by M. Pandolfi and R. Piva), pp. 275–282. Vieweg Verlag, Braunschweig (1984).
17. D. Gottlieb and S. A. Orszag, *Numerical Analysis of Spectral Methods: Theory and Application*, SIAM Monograph No. 26. SIAM, Philadelphia, PA (1977).
18. M. S. Engelman, *FIDAP, Fluid Dynamics Analysis Program Theoretical Manual*. Fluid Dynamics International Inc., Revision 5 (1990).
19. M. S. Engelman and R. L. Sani, *Proc. ASME Convection in Enclosures Conf.*, ASME HTD 26 (1983).

CONVECTION DANS UN CYLINDRE CHAUFFE DE FAÇON ASYMETRIQUE

Résumé—Dans des expériences de solidification dirigée (verticale) récentes, de la convection non-axisymétrique a été observée. Il fût montré que la particularité de l'écoulement est liée au manque de symétrie azimutale du champ de température à la paroi d'un cylindre vertical différentiellement chauffé. Motivé par ces observations nous avons examiné les conséquences de déviations azimutales apportées à un champ de température axisymétrique. Nous montrons que le degré d'asymétrie développé par l'écoulement dépend du rapport, A_θ, entre le maximum de différence de température azimutale et le maximum de différence de température verticale. Pour an valeur fixée de A_θ, ce degré d'asymétrie croît si on augmente les vitesses de l'écoulement (i.e. si on augmente le nombre de Rayleigh).

KONVEKTION IN EINEM ACHSENSYMMETRISCH BEHEIZTEN ZYLINDER

Zusammenfassung—Kürzlich wurde in vertikal ausgerichteten Erstarrungsexperimenten nicht-achsensymmetrische Konvektion beobachtet. Diese Erscheinung wurde so erklärt, daß die Asymmetrie durch einen Mangel von Symmetrie des aufgeprägten Temperaturfeldes in azimuthaler Richtung hervorgerufen wird, mit der Folge, daß die Symmetrie der Strömung mit zunehmender Geschwindigkeit kleiner wird. Diese Beobachtungen waren Anlaß für uns, die Auswirkungen nicht-achsensymmetrischer Wandtemperaturverteilungen in einem in vertikaler Richtung unterschiedlich beheizten Zylinder zu untersuchen. Es wird gezeigt, daß der Grad der Asymmetrie der Strömung vom Verhältnis A_θ zwischen den Amplituden der maximalen azimuthalen und vertikalen Temperaturunterschiede abhängt. Für einen festen Wert dieses Verhältnisses nimmt die Asymmetrie der Strömung mit wachsender Strömungsgeschwindigkeit (Rayleigh-Zahl) zu.

КОНВЕКЦИЯ В АСИММЕТРИЧНО НАГРЕВАЕМОМ ЦИЛИНДРЕ

Аннотация—В ранее проведенных экспериментах по вертикальному направленному затвердеванию наблюдалась неосесимметричная конвекция. Было сделано предположение, что асимметрия вызвана отсутствием азимутальной симметрии в задаваемой температуре и будет уменьшаться с ростом скоростей. В данной работе изучаются следствия отклонений от условий с осесимметричной температурой стенки в вертикальном цилиндре с неравномерным нагревом. Показано, что степень асимметрии течения зависит от отношения между амплитудами максимальных азимутальной и вертикальной разностей температур и при постоянном значении этого отношения асимметрия течения увеличивается с ростом скорости (числа Рэлея).